ELSEVIER

Journal of Alloys and Compounds 404–406 (2005) 545–549

Journal of ALLOYS AND COMPOUNDS

www.elsevier.com/locate/jallcom

Relationship between polymorphism and hydrogenation properties in $Ti_{0.64}Zr_{0.36}Ni$ alloy

F. Cuevas*, M. Latroche, A. Percheron-Guégan

LCMTR-ISCSA-CNRS, 2-8 rue Henri Dunant, 94320 Thiais Cedex, France

Received 25 August 2004; received in revised form 9 February 2005; accepted 14 February 2005
Available online 11 July 2005

Abstract

The influence of the parent crystal structure on the hydrogenation of $Ti_{0.64}Zr_{0.36}Ni$ alloy has been investigated. Austenitic $Ti_{0.64}Zr_{0.36}Ni$ alloy with cubic CsCl-type structure preserves its metal sublattice structure after hydrogenation. It forms $Ti_{0.64}Zr_{0.36}NiH_{1.6}$ hydride ($P_{H_2} = 1$ MPa and $T = 373$ K) through a cell-volume expansion of 10.4%. On the contrary, the monoclinic TiNi-type structure of martensitic $Ti_{0.64}Zr_{0.36}Ni$ alloy is modified after hydrogen absorption. At $P_{H_2} = 0.06$ MPa and $T = 373$ K, two hydrides coexist with orthorhombic CrB-type structure and compositions $Ti_{0.64}Zr_{0.36}NiH$ and $Ti_{0.64}Zr_{0.36}NiH_{2.2}$, which induces a cell-volume expansion of 5.36 and 18.3%, respectively. The stability of these crystal structures is discussed by comparison with other AB intermetallic compounds (A = Ti, Zr, Hf) and B = (Fe, Co, Ni).

Keywords: Intermetallics; Hydrogen storage materials; Crystal structure and symmetry; X-ray diffraction

1. Introduction

TiNi is an outstanding alloy due to both shape memory behavior and hydrogen uptake capability [1–4]. Its shape memory effect is allowed by a martensitic transformation (MT) between a high temperature phase of cubic symmetry and a low temperature phase of monoclinic symmetry [5,6]. MT is a first order and diffusionless reversible transition with thermal hysteresis. By analogy with steels, high and low temperature phases in TiNi are denoted as austenite and martensite, respectively. For equiatomic TiNi, the martensite starts to nucleate on cooling at $T \sim 310$ K, whereas the reverse transformation starts at $T \sim 340$ K [7]. Nevertheless, MT temperatures are strongly dependent on the chemistry (stoechiometry [7], metal substitutions [8] and impurity gas content [9]) and the thermo-mechanical history [10,11] of the alloy.

The crystal structure of TiNi austenite was determined long time ago [12]. It has a cubic CsCl-type structure (S.G. $Pm\bar{3}m$, Ni 1*a* (0, 0, 0), Ti 1*b* (1/2, 1/2, 1/2)) with lattice parameter $a = 3.015$ Å[13]. The crystal structure determination of TiNi martensite has been much problematic due to its complex structure and the difficulty of obtaining randomly oriented powder samples [14,15]. It is now widely accepted that its crystal structure is monoclinic $P2_1/m$ (Ti 2*e* (0.4176, 1/4, 0.2164), Ni 2*e* (0.0372, 1/4, 0.6752)) with lattice parameters $a = 2.898$ Å, $b = 4.108$ Å, $c = 4.646$ Å and $\beta = 97.78°$, as established by Kudoh et al. by single crystal X-ray diffraction [16].

Hydrogenation properties of TiNi austenite as refers to pressure–composition–isotherms (PCI) have been determined by Burch et al. [17]. TiNi absorbs up to 1.2 hydrogen atoms per AB unit formula (H/AB, A = Ti, B = Ni) at 400 K and 1 MPa of hydrogen pressure. H-absorption takes place without showing any evidence of a pressure invariant plateau region at $P > 0.02$ MPa. This may suggest that hydrogen enters as a solution phase, a statement that should be discarded after structural data of Noréus et al. [18] and Soubeyroux et al. [19]. In fact, hydrogen absorption induces a tetragonal distortion of the cubic alloy matrix forming a ($2a \times 4a$) supercell structure. Unit-cell parameters for $TiNiH_{1.4}$ hydride are reported to be $a = 6.2365$ Å and $c = 12.424$ Å, leading to a 10% cell-volume expansion with respect to the parent alloy. H-atoms almost occupy half of the octahedral Ti_4Ni_2 sites available in the metal sublattice.

* Corresponding author. Tel.: +33 1 4978 1225; fax: +33 1 4978 1203.
E-mail address: fermin.cuevas@glvt-cnrs.fr (F. Cuevas).

0925-8388/$ – see front matter © 2005 Elsevier B.V. All rights reserved.
doi:10.1016/j.jallcom.2005.02.072

As regards to the hydrogenation properties of TiNi martensite, scarce information is reported in the literature. This should be related to the difficulty of producing bulk specimens of martensitic-derived hydrides. The reasons of this are manifold. First, the martensitic phase only holds near or below room temperature, where H-diffusivity is sluggish. Secondly, TiNi alloy is extremely tough and, therefore, difficult to obtain in powder state for being hydrogenated in a reasonable time. Finally, solid–gas hydrogen absorption in TiNi alloy is easily hampered due to the formation of surface oxides. As a consequence, martensite hydrogenation has been mostly performed by electrochemical loading and the reported data only concerns modifications of the MT behavior in TiNi alloy by H-uptake [20–22]. Therefore, these studies do not provide fundamental results on the main hydrogenation properties (i.e., H-thermodynamics and hydride crystal structure) for the martensitic phase.

In this paper, we describe how the alloy crystal structure dictates the hydrogenation properties in the TiNi–H system. For such a study, Zr-substituted $Ti_{0.64}Zr_{0.36}Ni$ alloy has been used since it allows the hydrogenation of bulk martensitic alloy up to 400 K [23].

2. Experimental

Two Zr-substituted TiNi-type alloy ingots with nominal composition $Ti_{0.64}Zr_{0.36}Ni$ were elaborated by induction melting from the pure elements (purity 99.95%). The ingots were melted five times under secondary vacuum and turned over between each melting to ensure their homogeneity. One of them was subsequently annealed at 1273 K for 2 weeks under argon atmosphere. The second one was melt-spun under helium atmosphere over a stainless–steel wheel having a surface velocity of 19 m/s. This sample was obtained as a flat ribbon 40 μm in thickness. These two alloys will be referred to as "as-cast" and "melt-spun" alloys, respectively. Alloy composition was analyzed by electron probe microanalysis (EPMA) in a Cameca SX-100 instrument operated at 15 kV.

As concerns hydrogenation properties, solid–gas PCI curves for both alloys were obtained in a volumetric device at 373 K between 10^{-3} and 1 MPa of deuterium pressure. Deuterium was used instead of hydrogen to allow a latter neutron diffraction study that will be published elsewhere. However, for the sake of simplicity, the term "hydrogen" will be used in the following. Before hydrogenation, samples were chemically etched with 10%HF solution for 30 s to remove surface oxides. After PCI measurements, hydrided samples at selected concentrations were subsequently cooled to room temperature in order to study their crystal structure. As result of hydrogenation, as-cast alloy is rendered as fine powder, whereas melt-spun alloy is only embrittled.

Alloy crystal structures before and after hydrogenation were studied at room temperature by powder X-ray diffraction (XRD) using Cu Kα radiation in a θ–θ diffractometer (Bruker AXS D8Advance equipped with backscattered rear graphite monochromator). As mentioned before, powders from the starting alloys are difficult to obtain. To overcome this problem, alloy structures where studied from thermally degassed hydride samples. Desorption was performed under secondary vacuum up to 603 and 733 K for the "as-cast" and "melt-spun" alloys, respectively. XRD data were refined by the Rietveld method using the Fullprof program [24].

3. Results and discussion

EPMA analysis for the as-cast alloy shows a major phase (98%) of composition $Ti_{0.64(1)}Zr_{0.34(1)}Ni_{1.02(1)}$ and minor $(Ti,Zr)_2Ni$-type precipitates (2%). The melt-spun alloy is chemically homogeneous with composition $Ti_{0.656(2)}Zr_{0.350(2)}Ni_{0.994(2)}$.

XRD data for "as-cast" and "melt-spun" alloys are completely different as can be observed in Fig. 1. As a matter of fact, the "as-cast" alloy has a martensitic-type structure whereas the "melt-spun" alloy is of austenitic-type. This result is in agreement with previous DSC analysis showing that the "as-cast" alloy undergoes the reverse MT at 423 K, whereas no transformation is observed for the "melt-spun" alloy above room temperature [23]. As austenitic-type alloy is obtained by a non-equilibrium route, this phase is thought to be metastable at room temperature.

The results of Rietveld analysis for both alloys are summarized in Table 1. For "as-cast" alloy, besides the monoclinic martensite phase, two secondary phases are detected: an austenitic-type (Ti,Zr)Ni (6%) phase and $(Ti,Zr)_2Ni$ phase (7%). The increased amount of $(Ti,Zr)_2Ni$ phase (7%) as compared with that found by EPMA for the starting alloy (2%) is thought to be caused by minor oxygen contamination during the hydrogen absorption/desorption process. Oxygen is known to favor the formation of Ti_2NiO-type precipitates [9]. $Ti_{0.64}Zr_{0.36}Ni$ martensite has the same crystal symmetry as TiNi martensite [16]. Main effects of Zr-substitution are an expansion of the unit-cell-volume (8.5%) and the increase of

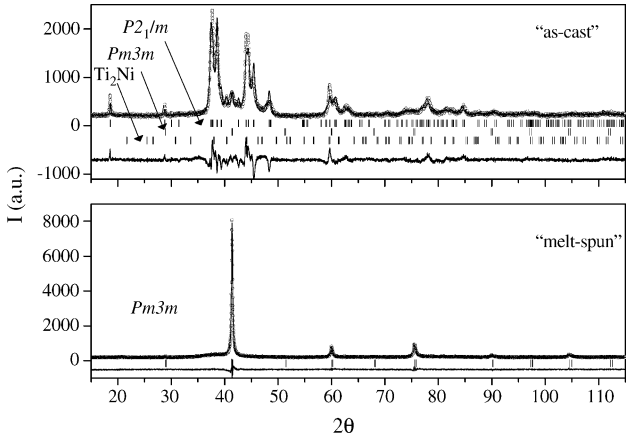

Fig. 1. XRD data and Rietveld analysis of "as-cast" and "melt-spun" $Ti_{0.64}Zr_{0.36}Ni$ alloys. Calculated diffraction pattern (continuous line), diffraction line positions (vertical bars) and difference curve at the same scale (below) are given.

Table 1
Structural data of "as-cast" and "melt-spun" $Ti_{0.64}Zr_{0.36}Ni$ alloys

"As-cast" $Ti_{0.64}Zr_{0.36}Ni$ AB alloy
SG = $P2_1/m$, $a = 3.0601(6)$ Å, $b = 4.0736(6)$ Å, $c = 4.9046(9)$ Å, $\beta = 103.75(1)^\circ$, V/AB = 29.74(1) Å^3
(Ti,Zr) 2*e* (0.375(1), 1/4, 0.210(5)), $B = 0.34(7)$ Å^{2}Ni 2*e* (0.077(1), 1/4, 0.670(5)), $B = 0.34(7)$ Å^2
secondary phases: $Pm3m$ – austenite-type (Ti,Zr)Ni: 6(1)%, $a = 3.084(1)$ Å, $Fd3m$ $(Ti,Zr)_2Ni$-type 7(1)%, $a = 11.611(4)$ Å
$R_{wp} = 11.2\%$, $R_p = 8.68\%$, $R_{B1} = 7.9\%$, $R_{B2} = 6.8\%$, $R_{B3} = 16.3\%$, $\chi^2 = 4.12$

"Melt-spun" $Ti_{0.64}Zr_{0.36}Ni$ AB alloy
SG = $Pm3m$, $a = 3.0781(2)$ Å, V/AB = 29.166(3) Å^3
(Ti,Zr) 1*b* (1/2, 1/2, 1/2), $B = 2.2(1)$ Å^2, Ni 1*a* (0, 0, 0), $B = 2.8(1)$ Å^2
$R_{wp} = 7.37\%$, $R_p = 5.90\%$, $R_B = 3.83\%$, $\chi^2 = 2.47$

Space group (SG), cell parameters (*a*, *b*, *c*, β), normalized cell-volume (V/AB), atomic coordinates (*x*, *y*, *z*), displacement factors (*B*) and reliability factors (R_{wp}, R_p, R_{Bi} for each phase, χ^2).

the monoclinic distortion (β-angle changes from 97.78° to 103.75°). As concerns to the "melt-spun" alloy, XRD data is well-fitted with a CsCl-type structure. Zr-substitution induces a cell-volume expansion of 6.4%. Cell-volume expansion in both austenitic and martensitic structures is due to the differences of atomic radii between Ti and Zr atoms ($r_{Ti} = 1.47$ Å and $r_{Zr} = 1.60$ Å).

PCI absorption curves at 373 K for both alloys are shown in Fig. 2 and were discussed in detail in previous publications [23,25]. "Melt-spun" austenitic alloy forms $ABH_{1.5}$ β-hydride at 1 MPa with no plateau pressure. On the contrary, "as-cast" martensitic alloy absorbs up to 2.6 H/AB at the same pressure while displaying a flat plateau pressure at 0.06 MPa. This plateau reveals the existence of two hydride phases (β and γ) with hydrogen concentrations of 1 and 2.2 H/AB, respectively. In order to study the crystal structures of the reported hydrides, each hydrided sample was cooled down to room temperature under hydrogen atmosphere (dotted lines in Fig. 2). Final concentration for the β-austenitic hydride is 1.60(5) H/AB and that of the β + γ-martensitic hydride is 1.8(1) H/AB. Last composition was chosen to obtain equal contribution to XRD data from both hydrides.

XRD data for both hydrided alloys are shown in Fig. 3 and the results of the Rietveld analysis are summarized in Table 2. As concerns to the "melt-spun" alloy, the metal sublattice

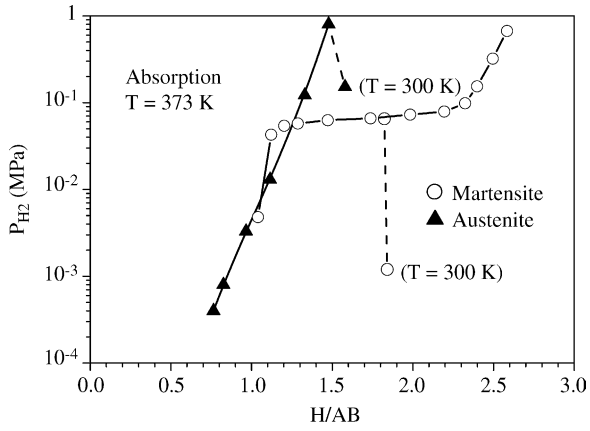

Fig. 2. PCI absorption curves at 373 K for martensite ("as-cast") and austenite ("melt-spun") $Ti_{0.64}Zr_{0.36}Ni$ alloys. P–C path on cooling to room temperature is shown by a dashed line.

preserves the CsCl-type structure upon hydrogenation. Contrary to binary TiNi alloy [19], no tetragonal distortion occurs, which may be related to the structural disorder induced by Zr-substitution. In fact, such disorder is reflected by the high displacement parameter *B*-value of Ni ($B_{Ni} = 5.5$ Å^2) that can be attributed to a random variation of the local con-

Table 2
Structural data of "as-cast" and "melt-spun" $Ti_{0.64}Zr_{0.36}Ni$ alloys after hydrogenation

Hydrided "as-cast" alloy, H/AB = 1.8
β-phase: 49(1)% SG = $Cmcm$, $a = 3.1577(6)$ Å, $b = 9.901(2)$ Å, $c = 4.0065(7)$ Å, V/AB = 31.31(1) Å^3, $\Delta V/V = 5.3\%$
(Ti,Zr) 4*c* (0, 0.149(1), 1/4), $B = 1.7(5)$ Å^{2}Ni 4*c* (0, 0.429(2), 1/4), $B = 3.2(1)$ Å^2
γ-phase: 51(1)% SG = $Cmcm$, $a = 3.2401(5)$ Å, $b = 10.287(2)$ Å,
$c = 4.2239(8)$ Å, V/AB = 35.20(1) Å^3, $\Delta V/V = 18.3\%$, (Ti,Zr) 4*c* (0, 0.144(1), 1/4), $B = 1.7(5)$ Å^{2}Ni 4*c* (0, 0.431(1), 1/4), $B = 2.1(1)$ Å^2
$R_{wp} = 7.59\%$, $R_p = 5.96\%$, $R_{B1} = 7.52\%$, $R_{B2} = 6.89\%$, $\chi^2 = 1.87$

Hydrided "melt-spun" alloy, H/AB = 1.6
β-phase: 100% SG = $Pm3m$, $a = 3.1812(2)$ Å, V/AB = 32.19(1) Å^3, $\Delta V/V = 10.4\%$
(Ti,Zr) 1*b* (1/2, 1/2, 1/2), $B = 1.6(1)$ Å^{2}Ni 1*a* (0, 0, 0), $B = 5.5(3)$ Å^2
$R_{wp} = 8.54\%$, $R_p = 6.68\%$, $R_B = 4.782\%$, $\chi^2 = 1.87$

Space group (SG), cell parameters (*a*, *b*, *c*), normalized cell-volume (V/AB), hydrogen-induced cell volume expansion ($\Delta V/V$), atomic coordinates (*x*, *y*, *z*), displacement factors (*B*) and reliability factors (R_{wp}, R_p, R_{Bi} for each phase, χ^2).

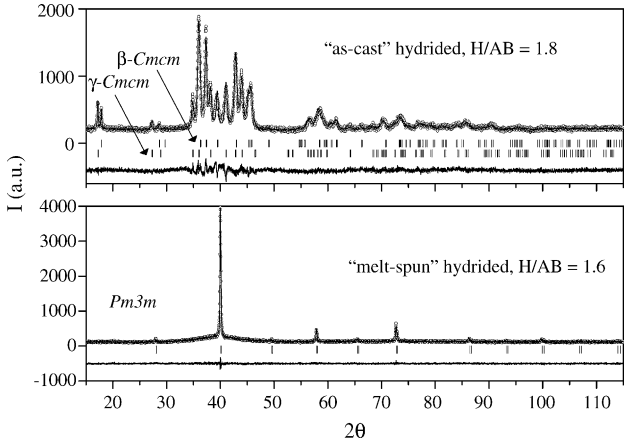

Fig. 3. XRD data and Rietveld analysis of "as-cast" and "melt-spun" $Ti_{0.64}Zr_{0.36}Ni$ alloys after hydrogenation. Calculated diffraction pattern (continuous line), diffraction line positions (vertical bars) and difference curve at the same scale (below) are given.

figuration of the neighboring Ti and Zr atoms around the Ni position. In addition, hydrogen uptake induces a cell volume expansion of 10.4% with respect to the $Ti_{0.64}Zr_{0.36}Ni$ alloy.

Diffraction data of the hydrided "as-cast" alloy is much complex. The monoclinic symmetry of the original alloy is modified since the XRD pattern is fully indexed with two orthorhombic CrB-type phases (S. G. *Cmcm*) having nearly equal contribution. Ni and Ti atoms occupy in both phases (denoted as β and γ) Wyckoff positions 4*c* $(0, y, 1/4)$ with $y_{Ti} \sim 0.145$ and $y_{Ni} \sim 0.430$. The main difference between β and γ phases lies in their lattice parameters and unit-cell-volume due to their distinct hydrogen contents. Normalized cell-volumes (V/AB) are 31.31 and 35.20 $Å^3$ for β and γ phases, respectively, which represents a cell-volume expansion as compared to H-free alloy of 5.3 and 18.3%. Therefore, a high discrete volume of expansion between β and γ phases occurs in the plateau region (13%), which can explain the decrepitation of the martensitic alloy after hydrogen charging. A more detailed description of the crystal structure, hydrogen location and composition of these phases, as obtained by conjoint refinement of XRD and neutron diffraction data, will be reported in a forthcoming paper.

To summarize, the crystal structures of $Ti_{0.64}Zr_{0.36}Ni$–hydrides are related to the parent structures of the alloy. The crystal symmetry of austenite is not modified during hydrogenation whereas, for martensite, it changes from monoclinic ($P2_1/m$) to base centered orthorhombic (*Cmcm*). However, this transformation can be easily achieved through a slight distortion of the beta angle in the parent alloy from 103.75° to 108.17°. To this respect, a recent study, based on density functional calculations, states that the stable structure of TiNi alloy at room temperature is *Cmcm*, being the monoclinic structure stabilized by residual internal stress [26].

It is amazing to note that the observed crystal structures of $Ti_{0.64}Zr_{0.36}Ni$ alloy and its hydrides gather all structures found in AB systems, where A belongs to IVB metal group (Ti, Zr, Hf) and B to the first row of VIIIB metals (Fe, Co, Ni) [27–31]. This is schematically displayed in Fig. 4. For the intermetallics, Fe- and Co-containing compounds crystallize in the CsCl-type structure, whereas Ni-containing compounds are CrB-type. For the hydrides, as refers to the metal sublattice, Ti-containing compounds tend to be CsCl-type, whereas Zr- and Hf-based compounds are CrB-type. These observations indicate that both electronic and lattice-size effects play a key role on the stabilization of a given structure. As a matter of fact, the increment of both the atomic electronic density (from Fe to Ni constituents) and the metal-atomic radii (from Zr to Hf constituents) favors AB alloy crystallization into the CrB-type structure. This tendency is confirmed by the sole effect of hydrogen absorption, which is capable by itself to transform CsCl- into CrB-type structure as occurs in ZrCo and HfCo compounds. TiNi alloy exhibits a crossover behavior as regards crystal stability between CsCl-

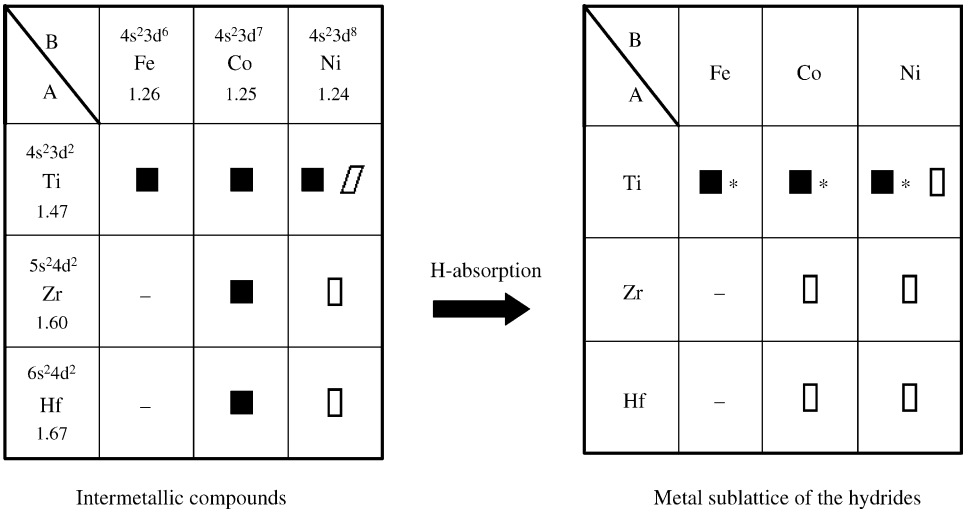

Fig. 4. Crystal structures of AB-type alloys (A = Ti, Zr, Hf; B = Fe, Co, Ni) before and after hydrogenation. FeZr and FeHf alloys do not exist as stable compound. Cubic, orthorhombic and monoclinic symmetries are represented by ■, □, and ◊ symbols, respectively. Outer-shell electronic configuration and atomic radii of the elements (Å) are given at the top and below the elements, respectively. (∗) Distorted CsCl-type structures.

and CrB-type structures, which is probably due to a compensation effect between the minor atomic radii of its constituents ($r_{Ni} = 1.24$ Å, $r_{Ti} = 1.47$ Å) and the highest electronic density of Ni ($4s^2 3d^8$ electronic outer shell configuration).

4. Conclusions

The martensitic transformation in TiNi-alloys is very sensitive to chemical modifications and thermo-mechanical treatments. This could be regarded either as a drawback to easily get reproducible results, or as a benefit to tailor the thermal stability of martensitic and austenitic phases as a function of sample composition and microstructure. This advantage was used for the synthesis of Zr-substituting TiNi alloy with either martensitic or austenitic structures at a given temperature. Thus, on one hand, by partial substitution of Ti by Zr, MT temperature is increased. This facilitates hydrogenation of the low-temperature monoclinic structure. On the other hand, by using a non-equilibrium technique such as melt-spinning, MT temperature is decreased and Zr-substituting TiNi alloy can be stabilized in the austenitic phase at room temperature. This procedure has allowed us determining the hydrogenation properties of austenitic and martensitic phases for the same chemical composition $Ti_{0.64}Zr_{0.36}Ni$. Both cubic and monoclinic structures absorb hydrogen reversibly with distinct crystallographic properties. The crystal symmetry of the parent cubic structure is preserved upon hydrogen absorption. Oppositely, the monoclinic structure transforms into two orthorhombic hydrides both having CrB-type structures, as occurs in the representative ZrNi intermetallic compound [29].

Acknowledgements

The authors wish to thank P. Ochin (CECM-CNRS, France) for the preparation of melt-spun samples, E. Leroy for EPMA analysis and F. Briaucourt for technical assistance.

References

[1] K. Otsuka, X. Ren, Intermetallics 7 (1999) 511.
[2] J. Van Humbeeck, Adv. Eng. Mater. 3 (2001) 837.
[3] E.W. Justi, H.H. Ewe, A.W. Kalberlah, N.M. Saridakis, M.H. Schaefer, Energy Conversion 10 (1970) 183.
[4] D. Fruchart, J.-L. Soubeyroux, S. Miraglia, S. Obbade, G. Lorthioir, F. Basile, D. Colin, F. Faudot, P. Ochin, A. Dezellus, Z. Phys. Chem. 179 (1993) 225.
[5] K. Otsuka, T. Sawamura, K. Shimizu, Phys. Status Solidi A 5 (1971) 457.
[6] G.D. Sandrock, A.J. Perkins, R.F. Heheman, Met. Trans. 2 (1971) 2769.
[7] J.-L. Murray (Ed.), ASM International, Metals Park, OH, 1987, p. 197.
[8] K.H. Eckelmeyer, Scripta Metall. 10 (1976) 667.
[9] P. Olier, F. Barcelo, J.L. Bechade, J.C. Brachet, E. Lefevre, G. Guenin, J. Phys. IV France 7 (1997) C5.
[10] Y. Liu, G.S. Tan, Intermetallics 8 (2000) 67.
[11] S. Miyazaki, Y. Igo, K. Otsuka, Acta Metall. 34 (1986) 2045.
[12] E. Dwight, Trans. AIME 215 (1959) 283.
[13] W. Bührer, R. Gotthardt, A. Kulik, O. Mercier, F. Staub, J. Phys. F: Met. Phys. 13 (1983) L77.
[14] G.M. Michal, R. Sinclair, Acta Cryst. B 37 (1981) 1803.
[15] R. Schmidt, M. Schlereth, H. Wipf, W. Assmus, M. Müllner, J. Phys.: Condens. Matter 1 (1989) 2473.
[16] Y. Kudoh, M. Tokonami, S. Miyazaki, K. Otsuka, Acta Metall. 33 (1985) 2049.
[17] R. Burch, N.B. Mason, J. Chem. Soc., Faraday Trans. I 75 (1979) 561.
[18] D. Noréus, P.-E. Werner, K. Alasafi, E. Schmidt-Ihn, Int. J. Hydrogen Energy 10 (1985) 547.
[19] J.-L. Soubeyroux, D. Fruchart, G. Lorthioir, P. Ochin, D. Colin, J. Alloys Compd. 196 (1993) 127.
[20] I.A. Stepanov, Y.M. Flomenblit, V.A. Zaymovskiy, Phys. Met. Metall. 55 (1983) 180.
[21] N. Wade, Y. Adachi, Y. Hosoi, Scr. Metall. Mater. 24 (1990) 1051.
[22] C. Damiani, J.L. Pelegrina, M. Ahlers, J. Alloys Compd. 284 (1999) 243.
[23] F. Cuevas, M. Latroche, P. Ochin, A. Dezellus, J.-F. Fernandez, C. Sanchez, A. Percheron-Guégan, J. Alloys Compd. 330–332 (2002) 250.
[24] J. Rodríguez-Carvajal, Physica B 192 (1993) 55.
[25] F. Cuevas, M. Latroche, P. Ochin, A. Dezellus, A. Percheron-Guégan, J. Alloys Compd. 356–357 (2003) 730.
[26] X. Huang, G.J. Ackland, K.M. Rabe, Nat. Mater. 2 (2003) 307.
[27] A.V. Irodova, V.A. Somenkov, S.S. Shil'shtein, L.N. Padurets, A.A. Chertkov, Sov. Phys. Crystallogr. 23 (1978) 591.
[28] R.M. Van Essen, K.H.J. Buschow, J. Less-Common Met. 64 (1979) 277.
[29] D.G. Westlake, J. Less-Common Met. 75 (1980) 177.
[30] P. Fischer, J. Schefer, K. Yvon, L. Schlapbach, T. Riesterer, J. Less-Common Met. 129 (1987) 39.
[31] J.S. Cantrell, R.C. Bowman Jr., J. Less-Common Met. 130 (1987) 69.